Modeling of microstructure evolution in regular eutectic growth

M. F. Zhu* and C. P. Hong†
Center for Computer-Aided Materials Processing (CAMP), Department of Metallurgical Engineering, Yonsei University, Shinchon-dong 134, Seodaemun-ku, Seoul 120-749, Korea
(Received 6 May 2002; published 30 October 2002)

The growth morphology of regular eutectics has been studied using a model eutectic alloy and a transparent $CBr_4-C_2Cl_6$ eutectic alloy. A modified cellular automaton (MCA) model is developed to model the evolution of regular eutectic microstructures. Different from the classical cellular automata in which only the temperature field is involved, the present model also includes the solute redistribution and the curvature effect during eutectic solidification. The finite-volume method, which is coupled with the cellular automaton model, is used to calculate the solute field in the calculation domain. The growth velocities of both eutectic phases are evaluated according to the local undercooling, consisting of thermal, solutal, and curvature undercoolings. The cooperative and competitive growth mechanisms of two eutectic phases are embedded in the present MCA model. The effects of diffusion and growth velocity on eutectic growth morphology, such as lamellar spacing and interface shape, were systematically investigated. The simulation results reveal a wide range of realistic eutectic growth features, such as eutectic oscillatory growth, selection of eutectic lamellar spacing accomplished by lamellar branching or lamellar termination, as well as interaction between the solute redistribution and the adjustment of volume fractions.

DOI: 10.1103/PhysRevB.66.155428 PACS number(s): 81.30.−t, 07.05.Tp, 81.10.Fq

I. INTRODUCTION

Precise understanding of the evolution of eutectic microstructures is crucial in controlling solidification of eutectic alloys. The growth behaviors of eutectic alloys have long received considerable attention since eutectic microstructures are of special interest not only from a theoretical point of view in terms of pattern formation and growth mode selection during solidification, but also from a practical point of view recognizing the properties associated with microstructures.[1,2]

Two important parameters of eutectic microstructures, markedly affecting the properties of materials, are the relative volume fractions of the two phases and interlamellar spacing. These parameters can be easily controlled by experiments. Generally, the volume fractions can be controlled to some extent by alloy compositions, whereas eutectic interlamellar spacing can be mainly controlled by growth velocity.[3,4] Extensive theoretical and experimental studies[5–9] have been carried out to investigate eutectic growth morphology and to provide models describing the eutectic microstructural characteristics as functions of alloy compositions and growth conditions. Following the pioneering analysis of Jackson and Hunt,[10] various theoretical models have been developed to relate eutectic interlamellar spacing with growth conditions.[11–13]

Numerical modeling has recently emerged as a powerful and important tool to simulate microstructural evolution during various solidification processes.[14–21] Some researchers have applied Monte Carlo (MC) models,[2,22] phase field models[23–25] and other numerical approaches, such as the boundary integral method,[26] to model the directional growth of lamellar eutectics and to exhibit a wide variety of characteristic features of eutectic formation. However, Monte Carlo techniques have the drawbacks of being unable to describe the time evolution of eutectic growth, due to the fact that the MC time step used in MC calculation is not correlated with real time. Meanwhile, the boundary integral method allows the reliable simulation of the dynamics of the solid/liquid interface and some basic eutectic lamellar instabilities such as oscillatory and tilted eutectic morphologies in a relevant low velocity regime, but it cannot handle catastrophic dynamic events such as the merging and branching of lamellae.[26] Furthermore, both Monte Carlo and boundary integral approaches cannot describe variations of the nonequilibrium solute field in liquid during eutectic solidification. On the other hand, phase field simulations effectively duplicate many experimental phenomena, such as eutectic lamellar spacing and volume fraction adjustments.[23–25] However, up to now phase field models are limited to a very small calculation domain due to a cell size limitation and a considerable computational power requirement.

The purpose of the present work, as a series of studies on the modeling of eutectic growth,[27,28] is to develop a modified cellular automaton (MCA) model for modeling microstructure evolution in eutectic solidification. Two kinds of eutectic alloys were examined: a model eutectic alloy with two solid phases of identical physical properties and a transparent CBr_4-C_2Cl_6 eutectic alloy. The effects of solute diffusion and growth velocity on eutectic growth morphology, such as eutectic lamellar spacing and interface shape, were investigated. Some of the computational results were verified by the experimental observations found in the literature.

II. MODEL DESCRIPTION AND NUMERICAL METHODS

A. Cooperative and competitive eutectic growth

In a nonfaceted/nonfaceted eutectic system, two thermodynamically distinct solid phases, labeled α and β, can simultaneously grow from the parent liquid phase when its temperature goes below the eutectic temperature, i.e., $L \rightarrow \alpha+\beta$, frequently forming a regular periodic structure of

 ©2002 The American Physical Society

lamellae. During eutectic solidification, two solutes are rejected into the liquid. Solute A accumulates in front of the β lamellae, while solute B accumulates in front of the α lamellae. The solute diffuses along the solid/liquid interface from one phase to the other. Consequently, solute diffusion plays a critical role in determining eutectic microstructural characteristics. As the lamellar spacing decreases, the solute buildup in front of the solid/liquid interface decreases. In other words, solute diffusion tends to decrease lamellar spacing. However, if the effect of solute diffusion on lamellar spacing is exclusively considered, lamellar spacing would be estimated to be much finer than the actual. Since excess free energy is associated with phase boundaries, as the lamellar spacing becomes finer, more surface area between the two phases is created for a unit volume of eutectic transformation. Thus, surface energy acts to increase lamellar spacing.[3,29] Under a certain growth condition, there must be an optimum lamellar spacing with respect to solute diffusion and surface energy considerations. If the lamellar spacing departs from the optimum, the thermodynamic equilibrium condition for the solid/liquid interface can no longer be fulfilled. This causes the adjustment of lamellar spacing by the creation of extra lamellae or terminations until the new lamellar spacing becomes stable. Accordingly, the key aspects for the modeling of eutectic growth should include the contributions of both solute diffusion and surface energy, which determine the cooperative and competitive eutectic growth behaviors, respectively.

In order to model eutectic growth, a two-dimensional calculation domain consisting of a uniform orthogonal arrangement of cells was considered. At the beginning of simulation, the whole domain was filled with liquid cells having a uniform eutectic composition. Two kinds of temperature fields in the calculation domain were considered: (i) a uniform temperature field with a certain thermal undercooling $\Delta T = T_E - T_0$, where T_E and T_0 are the eutectic and isothermal temperatures, respectively, and (ii) a temperature field imposed with a certain thermal gradient inside the domain. Directional eutectic growth was considered to occur from the bottom of the calculation domain, where a row of α and β seeds was assigned according to the equilibrium volume fraction of two eutectic phases and various initial lamellar spacings. The seeds of phases α and β have their crystallographic orientation of $0°$ with respect to the vertical growth direction.

During eutectic solidification, the driving force for eutectic transformation is defined by the local undercooling ΔT, which consists of four contributions:

$$\Delta T = \Delta T_T + \Delta T_C + \Delta T_r + \Delta T_k, \tag{1}$$

where ΔT_T is thermal undercooling, ΔT_C is solutal undercooling, ΔT_r is curvature undercooling, and ΔT_k is kinetic undercooling. For most regular eutectic systems, it is generally considered that kinetic undercooling is negligible.[30] Therefore, the total local undercooling at the solid/liquid interface at time t_n, $\Delta T(t_n)$, is considered to be the sum of three contributions, given by

$$\Delta T(t_n) = T_E - T(t_n) + m_i \cdot [C(t_n) - C_E] - \Gamma_i \overline{K}_i(t_n), \tag{2}$$

where T_E and C_E are, respectively, the eutectic temperature and the eutectic composition. Γ_i is the Gibbs-Thomson coefficient of phase i (phase α or β). $\overline{K}_i(t_n)$, $C(t_n)$, and $T(t_n)$ are the mean curvature with respect to phase i, and the concentration and the temperature of a liquid cell at the solid/liquid interface at time t_n, respectively. The liquidus slope m_i is negative for the α-phase growth and positive for the β-phase growth, i.e., $m_\alpha < 0$ and $m_\beta > 0$.

According to an analytical model,[30] the relationship between the growth velocity of eutectics and the interface undercooling can be expressed as

$$v[\Delta T(t_n)] = a \cdot \Delta T(t_n)^2, \tag{3}$$

where a is the growth kinetics coefficient, which is chosen to be 10^{-5} m/sK^2.

Once a cell has nucleated or solidified, it will grow with a growth velocity determined by local undercooling. At a certain time t_n, the growth length of a solidified cell at the solid/liquid interface, $l(t_n)$, is given by

$$l(t_n) = (\cos\theta + |\sin\theta|)^{-1} \left(\sum_{n=1}^{N} v[\Delta T(t_n)] \times \Delta t_n \right), \tag{4}$$

where Δt_n is the time step, θ is the angle of the preferential growth direction of a solid cell with respect to the linking line between this solid cell and its neighboring liquid cell, and N indicates the iteration number. Then, the solid fraction of a given cell at a certain time, $f_s(t_n)$, can be expressed by

$$f_s(t_n) = \frac{l(t_n)}{L}, \tag{5}$$

where L is the cell spacing. When $f_s(t) \geqslant 1$, the neighboring liquid cell is captured by the solid cell and its state changes from liquid to solid. The detailed growth algorithm of a nonfaceted crystal can be found elsewhere.[19]

It is to be noted that the liquidus slope m_i in Eq. (2) is negative for the α-phase growth and positive for the β-phase growth. The Gibbs-Thomson coefficients and the interface mean curvatures for phases α and β are also different. The local undercooling taken from the center of an interface liquid cell is thus different with respect to the solidification of phases α and β. Therefore, if an interface liquid cell is neighbored by both the α and β phase cells, local undercoolings and growth lengths with respect to the growth of phases α and β are calculated and compared simultaneously. The competitive eutectic growth mechanism is thus directly embedded in the present MCA growth algorithm.

As described previously, the balance between solute diffusion and surface energy, i.e., solutal and curvature undercoolings, is one of the most important mechanisms controlling eutectic growth. A stable eutectic microstructure forms when proper diffusion coupling is maintained between phases α and β. If lamellar spacing increases, the lateral diffusion distance between lamellae increases, resulting in insufficient diffusion and giving rise to the piling up of excess solute in front of the wider α phase. Thus, the α lamel-

TABLE I. Physical properties used in the present simulation.

Symbol	Definition and units	Model alloy	$CBr_4-C_2Cl_6$[a]
T_E	eutectic temperature (K)	356.0	356.0
m_α	liquidus slope of α phase (K/wt %)	-0.5	-1.48
m_β	liquidus slope of β phase (K/wt %)	0.5	2.16
C_E	eutectic composition (wt %)	8.4	8.4
C_α^0	solubility limit of α phase (wt %)	5.08	5.08
C_β^0	solubility limit of β phase (wt %)	16.18	16.18
f_α	volume fraction of α phase (—)	0.676	0.676
f_β	volume fraction of β phase (—)	0.324	0.324
Γ_α	Gibbs-Thomson coefficient of α phase (mK)	1.5×10^{-7}	0.8×10^{-7}
Γ_β	Gibbs-Thomson coefficient of β phase (mK)	1.5×10^{-7}	1.14×10^{-7}
D_l	solute diffusion coefficient in liquid (m^2/s)	1.0×10^{-9}	1.24×10^{-9}

[a]Reference 32.

lae have a negative curvature in the middle, leading to branching by the nucleation of phase β in the concave regions and the growth of newly nucleated β crystals, thereby reducing lamellar spacing to recover stable growth. The present model takes into account this mechanism about lamellar spacing reduction, which involves the nucleation and the growth of phase β in the solute enriched pockets associated with the concave regions of the α lamellae. A β nucleus is introduced in front of the α lamellae when the following two conditions are satisfied simultaneously: (i) The liquid/α interface mean curvature is negative, i.e., $\overline{K}_\alpha(t_n)<0$. (ii) The departure of concentration from the eutectic composition is larger than 1.8, i.e., $\Delta C=C_i-C_E>1.8$. Thus, the branching of lamellae is generated and the cooperative growth of eutectics is maintained.

B. Interface mean curvature

The mean curvature of an interface cell at time t_n with a solid fraction of $f_s(t_n)$ can be calculated using a counting-cell method[31] as follows:

$$\overline{K}_i=\frac{1}{\Delta a}\left[1-\frac{2}{n+1}\left(f_s(t_n)+\sum_{j=1}^{n} f_{s,i}(j)\right)\right], \tag{6}$$

where $\Delta a=\Delta x=\Delta y$ is the cell size, $f_{s,i}(j)$ is the solid fraction of phase i of the neighboring cells, and n is the number of neighboring cells around this interface cell. In the present simulation n is equal to 8, which indicates the number of neighboring cells of the first layer. The values of the curvature calculated by Eq. (6) vary from $1/\Delta a$ to 0 for convex interfaces and from 0 to $-1/\Delta a$ for concave interfaces. If an interface liquid cell is neighbored by both α and β solid phases, the mean curvatures with respect to phases α and β, $\overline{K}_\alpha$ and $\overline{K}_\beta$, should be calculated respectively.

C. Solute redistribution

The assumptions for solute redistribution during eutectic solidification are as follows:

(i) The solidified α and β phases preserve the equilibrium composition, i.e., $L\rightarrow\alpha(C_{\alpha0})+\beta(C_{\beta0})$.

(ii) The solute field during eutectic solidification is primarily controlled by diffusion in liquid, and no considerations of diffusion in solid and convective mass transfer are taken into account.

As the eutectic solidification proceeds, a solidified α-phase cell rejects the solute atoms to its neighboring liquid cells, i.e., $\Delta C=C_l-C_{\alpha0}$. Conversely, a solidified β-phase cell will absorb the solute atoms from its neighboring liquid cells, i.e., $\Delta C=C_l-C_{\beta0}$. Diffusion within the liquid region was simulated by the finite-volume method. The governing equation for solute redistribution in liquid is given by

$$\frac{\partial C_l}{\partial t}=D_l\cdot\nabla^2 C_l+(C_l-C_{\alpha0})\frac{\partial f_{s,\alpha}}{\partial t}+(C_l-C_{\beta0})\frac{\partial f_{s,\beta}}{\partial t}, \tag{7}$$

where t is time and D_l is the solute diffusion coefficient in liquid. $C_{\alpha0}$, $C_{\beta0}$, $f_{s,\alpha}$, and $f_{s,\beta}$ are the solubility limits and the solid fractions of phases α and β, respectively. The second and third terms on the right-hand side of Eq. (7) indicate

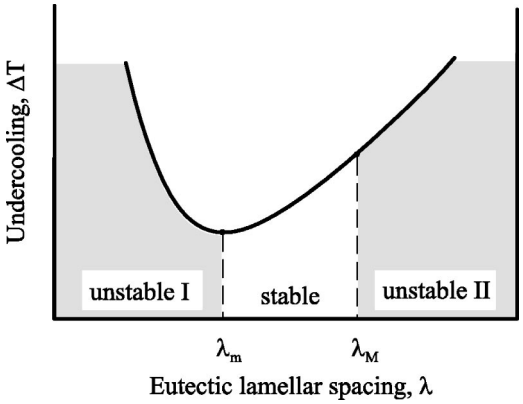

FIG. 1. A schematic plot of the relationship between average interface undercooling and eutectic lamellar spacing at a constant growth velocity, indicating the regions of stable and unstable lamellar spacing, as predicted by the JH model (Ref. 10) ($\Delta T=K_1\lambda V+K_2/\lambda$).

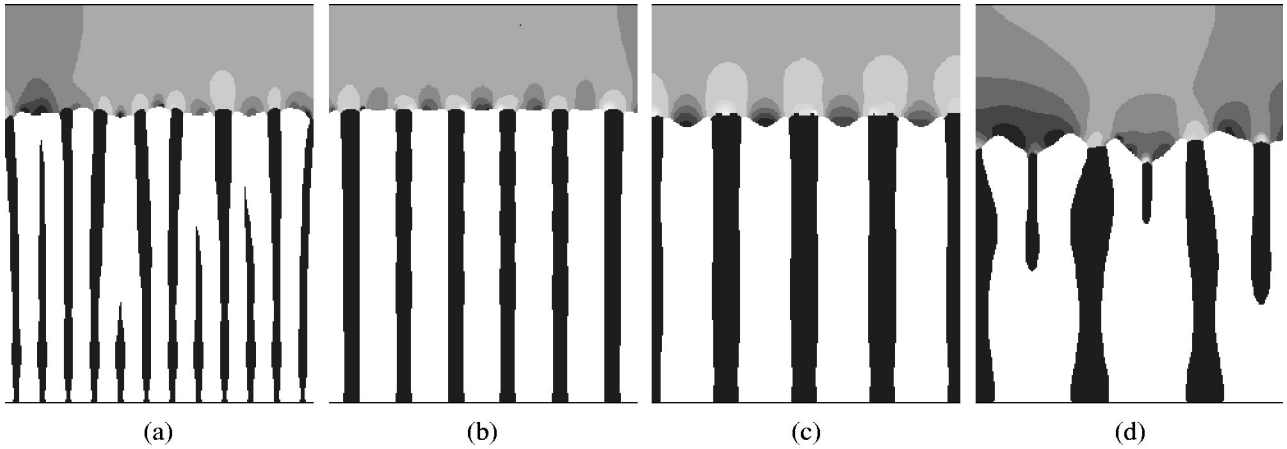

FIG. 2. The simulated lamellar eutectic microstructures with a growth velocity of 1.5 μm/s and various initial lamellar spacings (a) $\lambda = 15$ μm, (b) $\lambda = 25$ μm, (c) $\lambda = 38$ μm, and (d) $\lambda = 55$ μm.

the solute gain and loss resulting from the generation of eutectic solid fractions at the solid/liquid interface, respectively.

An explicit difference scheme was applied for calculating the solute diffusion, and the zero-flux boundary conditions were used for the cells located on the boundary of the calculation domain. The physical properties used in the present calculation are listed in Table I.

III. RESULTS AND DISCUSSION

A. Selection of eutectic lamellar spacing at a fixed growth velocity

The dominant variables of eutectic solidification are the undercooling ΔT, the growth velocity V, and the lamellar spacing λ.[29] Jackson and Hunt[10] (JH) developed an analytical model to relate eutectic lamellar spacing with growth rate in the directional solidification of regular eutectic alloys. According to their model, eutectic lamellar spacing is given as a function of undercooling and growth rate as follows:

$$\triangle T = K_1 \lambda V + K_2/\lambda, \tag{8}$$

where K_1 and K_2 are the constants for a given alloy system.

The relationship between lamellar spacing and interface undercooling at a fixed growth rate, as predicted by Eq. (8), is illustrated schematically in Fig. 1. Figure 1 also indicates that a finite band of stable eutectic lamellar spacings exists for a given growth velocity. This basic idea of eutectic stability has been extensively examined by a number of experimental studies. The results show that in directional solidification of regular eutectic alloys, the system will select the lamellar spacing giving a minimum undercooling at the interface, which is denoted by λ_m in Fig. 1.[4]

The present model was applied to simulate the eutectic growth morphology using a model eutectic alloy. As shown in Table I, the model alloy has the same eutectic temperature, eutectic composition, and solubility limits of both phases α and β as those of the transparent organic $CBr_4 - C_2Cl_6$ eutectic alloy. However, other physical properties are assumed to be identical, i.e., $m_\alpha = -m_\beta$ and $\Gamma_\alpha = \Gamma_\beta$. The stability of the eutectic front will thus not be biased by the differences in the physical properties of phases α and β. The calculation domain consists of 300×380 cells with a cell size of 0.5 μm. Figure 2 indicates the simulated eutectic microstructures at a fixed growth velocity of 1.5 μm/s with various initial lamellar spacings $\lambda = 15$ μm, 25 μm, 38 μm, and 55 μm. The white color represents phase α and the black

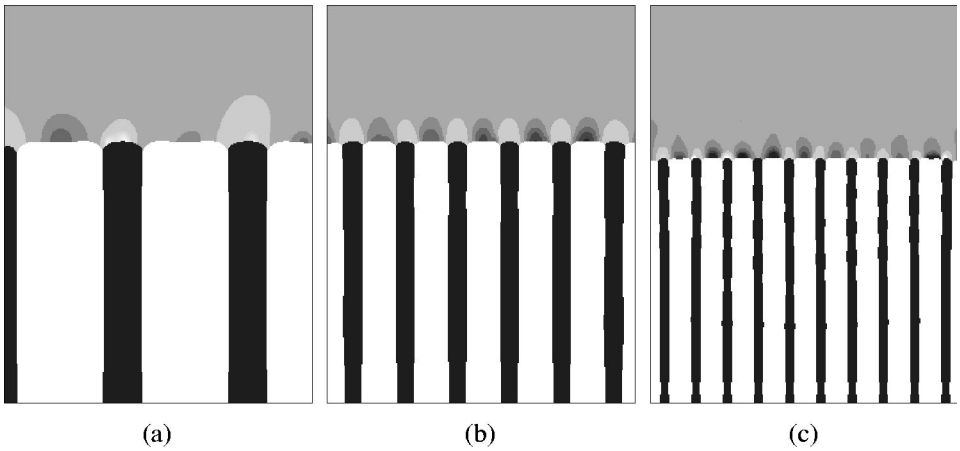

FIG. 3. The effect of diffusion on the stable lamellar spacing: (a) $D_l = 5.0 \times 10^{-9}$ m^2/s, (b) $D_l = 1.0 \times 10^{-9}$ m^2/s, and (c) $D_l = 0.22 \times 10^{-9}$ m^2/s.

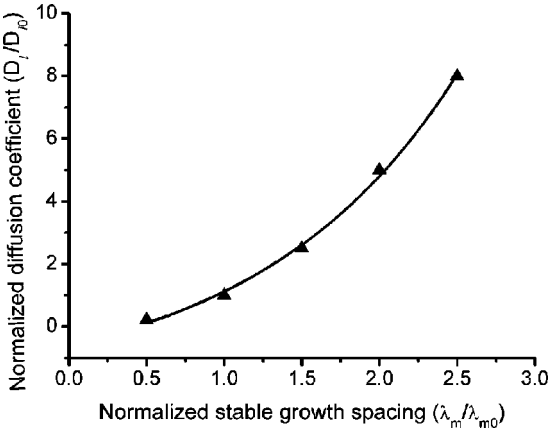

FIG. 4. The relationship between normalized solute diffusion coefficient and normalized stable growth spacing (normalized factors: $D_{l0}=1.0\times10^{-9}$ m^2/s and $\lambda_{m0}=30$ μm).

phase β. The gray color ahead of the solid/liquid interface represents the nonequilibrium solute field in the liquid: the darker the color, the higher the solute concentration. It can be noted from Fig. 2 that there exists a region of solute-enriched liquid ahead of phase α due to the rejection of solute at the α/liquid interface, and a region of solute-depleted liquid ahead of phase β. As eutectic growth proceeds, some lamellae are eliminated in the case of $\lambda=15$ μm. When a β lamella is eliminated, the adjacent α lamellae join together to form a single α lamellar, which generally reduces its thickness in relation to the thickness of the adjoining β lamellae in order to maintain the ratio of the volume fraction of the α and β phases at a constant value. These termination events lead to an increase in the lamellar spacing as shown in Fig. 2(a), which belongs to the unstable region I in Fig. 1. When the eutectic lamellar spacing is 25 μm, the lamellae organize themselves into a nearly uniform array as shown in Fig. 2(b), and hence this lamellar spacing can be considered as $\lambda=\lambda_m$. As the lamellar spacing becomes larger than λ_m as shown in Fig. 2(c), the insufficient solute diffusion yields a large accumulation of solute in front of α lamellae, developing solute enriched concave hollows at the center of the α/liquid interface. At an initial lamellar spacing of $\lambda=55$ μm, which is larger than the maximum stable lamellar spacing denoted as λ_M, eutectic growth becomes unstable followed by nucleation and growth of phase β at the center of phase α, leading to a decrease of original lamellae as shown in Fig. 2(d). The simulation results in Fig. 2 also exhibit that when the lamellar spacing is $\lambda<\lambda_m$, the predominant factor responsible for eutectic instability is the curvature effect, whereas the unstable growth of region II is primarily caused by solute insufficient diffusion. When a lamellar spacing λ is equal to the optimum lamellar spacing λ_m at a certain growth velocity, the effects of diffusion and curvature balance. Figure 2 provides visual evidence of the selection of lamellar spacing predicted by the analytical models and experimental observations.

In order to further examine the effect of solute diffusion on eutectic lamellar spacing, a simulation was carried out with various solute diffusion coefficients. Figure 3 represents the effect of solute diffusion on the stable eutectic lamellar spacing: (a) $D_l=5.0\times10^{-9}$ m^2/s, (b) $D_l=1.0\times10^{-9}$ m^2/s, and (c) $D_l=0.22\times10^{-9}$ m^2/s. It is obvious that a decrease in the diffusion coefficient will lead to an increase of solute departure from the eutectic composition, $\triangle C=|C_i-C_E|$, ahead of the solid/liquid interface. According to Eq. (2), an increase of $\triangle C$ results in an increase of the solute diffusion effect. The eutectic stable lamellar spacing λ_m thus becomes finer as shown in Figs. 3(a) through 3(c). The relationship between normalized diffusion coefficients and normalized stable lamellar spacing is shown in Fig. 4, exhibiting a monotonous increase of eutectic stable lamellar spacing with solute diffusion coefficient. The calculation conditions of Figs. 3 and 4, such as the calculation domain and the cell size, are the same as those of Fig. 2.

B. Eutectic oscillatory growth

Eutectic oscillatory instabilities have also been commonly observed experimentally in eutectic growth.[26] In order to predict the eutectic oscillatory growth mode, the calculation domain was divided into 440×420 cells with a cell size of 0.05 μm. The interface thermal undercooling was set to be

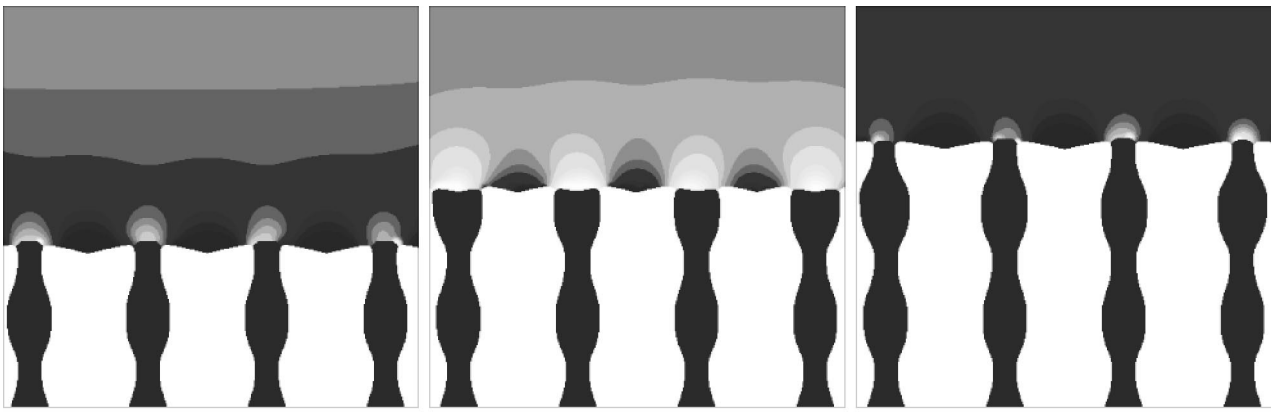

FIG. 5. The interaction between solute redistribution and volume fraction adjustment: (a) $t=0.1$ s, $\lambda_\alpha/\lambda>f_\alpha$, $\overline{C_l}>C_E$, (b) $t=0.13$ s, $\lambda_\alpha/\lambda<f_\alpha$, $\overline{C_l}<C_E$, and (c) $t=0.16$ s, $\lambda_\alpha/\lambda>f_\alpha$, $\overline{C_l}>C_E$.

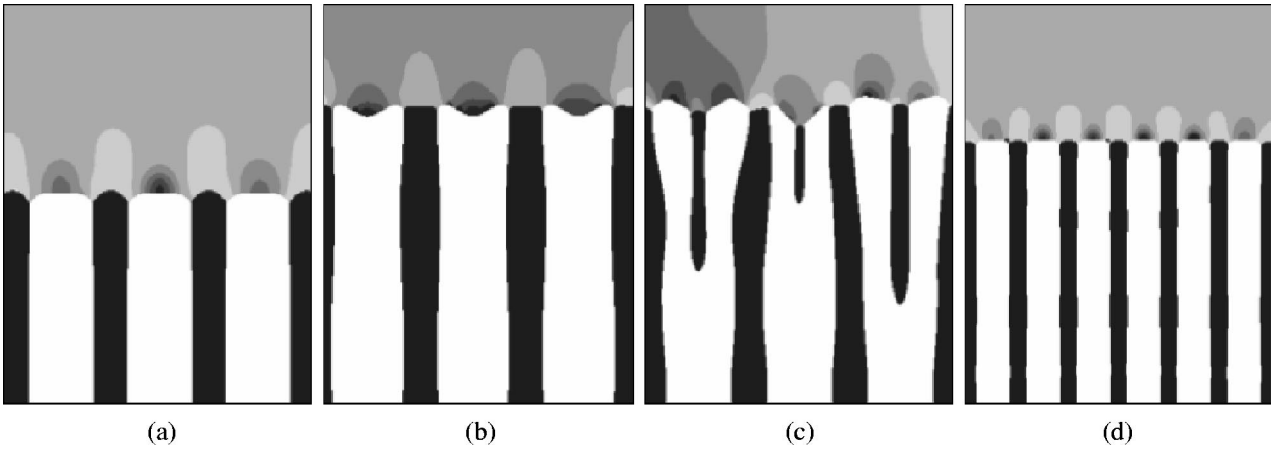

FIG. 6. The simulated lamellar eutectic microstructures with an increase of growth velocity: (a) $v=10$ μm/s, (b) $v=20$ μm/s, (c) $v=28$ μm/s, and (d) $v=35$ μm/s.

1.4 K. Figure 5 indicates the simulated evolution of eutectic oscillatory morphology. It is observed from Fig. 5(a) that at $t=0.1$ s , the volume fraction of phase α is larger than the equilibrium volume fraction of phase α, i.e., $\lambda_\alpha/\lambda > f_\alpha$, leading to the average liquid concentration in front of the solid/liquid interface higher than the eutectic composition, i.e., $\overline{C_l} > C_E$. According to Eq. (2), the departure of the average solid/liquid interface composition from C_E, $\triangle C = \overline{C_l} - C_E$, is proportional to the growth undercooling. Because the liquidus slopes of phases α and β are given as $m_\alpha < 0$ and $m_\beta > 0$, $\triangle C > 0$ will result in that the driving force for the growth of β lamellae is larger than that of α lamellae, which automatically adjusts the volume fraction by increasing the β lamellar width and decreasing the α one. Therefore, at $t=0.13$ s, an inverse situation takes place, i.e., $\lambda_\alpha/\lambda < f_\alpha$ and $\overline{C_l} < C_E$ as shown in Fig. 5(b). This will result in an increase of the volume fraction of phase α and a decrease of phase β. At $t=0.16$ s, the same situation as Fig. 5(a) occurs as shown in Fig. 5(c). This kind of timely periodic motions of the interface yields the eutectic oscillatory microstructures. Accordingly, the appearance of the oscillatory morphology can be explained physically by considering the destabilizing effect of the solute field ahead of the solid/liquid interface. The phenomena shown in Fig. 5 are consistent with the experimental observations and the simulation results of a phase field model and a boundary integral technique.[25,26] Moreover, Fig. 5 provides clearer evidence for a strong interaction between solute redistribution in liquid and volume fraction adjustment, which is the dominant mechanism controlling eutectic oscillatory growth.

C. The effect of growth velocity on lamellar spacing selection

In order to investigate the effect of growth velocity on lamellar spacing selection in directional solidification, a simulation by the MCA model was carried out in a calculation domain consisting of 400×520 cells with a cell size of 0.1 μm. Different interface thermal undercoolings were imposed to control eutectic growth velocity. Figure 6 shows the simulated eutectic microstructures of a transparent organic $CBr_4-C_2Cl_6$ alloy with various growth velocities $v=10$ μm/s, 20 μm/s, 28 μm/s, and 35 μm/s. It is to be noted that there is a strong interaction between solute redistribution and eutectic phase transformation. The eutectic lamellar spacing and the interface shape are controlled by the imposed growth rate. With a low growth velocity of $v=10$ μm/s, two solid phases advance in a steady-state fashion and form a periodic structure of lamellae with a relatively large lamellar spacing, as shown in Fig. 6(a). When the growth velocity increases, the solute supersaturation in front of lamellae increases, resulting in the development of a deep depression in front of α lamellae, followed by the nucleation of β crystals in these concave regions in the center of the α lamellae and the subsequent growth of the newly nucleated β phase. This will eventually stabilize the eutectic growth with a finer lamellar spacing, as shown in Figs. 6(b) through 6(d). Conversely, Fig. 7 illustrates the changes in eutectic lamellar spacing and interface morphology caused by the decrease in growth velocity $v=40$ μm/s, 30 μm/s, 25 μm/s, and 15 μm/s. It can be noted that with a growth velocity of $v=40$ μm/s, eutectic growth with a fine lamellar spacing exhibits a uniform periodic array as shown in Fig. 7(a). As growth velocity decreases, eutectic instability, which is caused by the curvature effect, provokes the volume fraction adjustment due to the annihilation of lamellae through competitive overgrowth by their neighbors, as shown in Fig. 7(b). In the case of Fig. 7(c), eutectic growth can be stable, but there is a concave α/liquid interface with enriched solute due to a slight insufficient solute diffusion. With a further decrease in growth velocity, the new spacing becomes stable with respect to solute diffusion and the curvature effect, and eutectic growth can be adjusted, as shown in Fig. 7(d).

The effect of growth velocity on steady-state eutectic lamellar spacing was also simulated and compared with the experimental observations found in the literature.[4] Figure 8 indicates the typical steady state eutectic microstructures of $CBr_4-8.4\,wt\,\%C_2Cl_6$ directionally solidified at a temperature gradient of 3.6 K/mm with various growth velocities 0.2 μm/s, 0.5 μm/s, and 1.0 μm/s. The figures in the left column indicate the simulated eutectic microstructures and

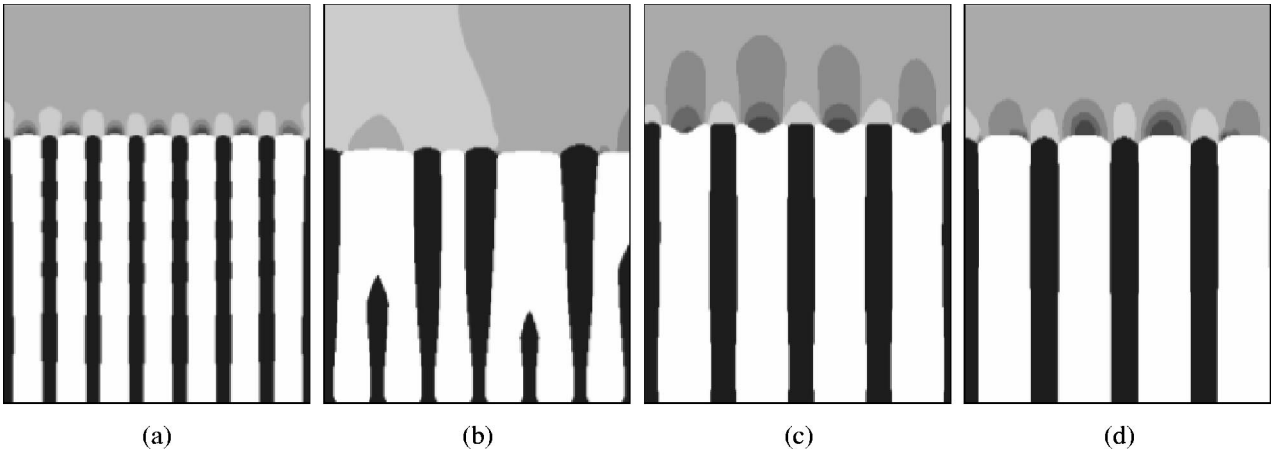

FIG. 7. The simulated lamellar eutectic microstructures with a decrease of growth velocity: (a) $v=40$ μm/s, (b) $v=30$ μm/s, (c) $v=25$ μm/s, and (d) $v=15$ μm/s.

the ones in the right the experimental results.[4] The calculation domain consists of 450×180 cells with a cell size of 2 μm. It can be seen that the solid-liquid interface remains planar for these three velocities. However, the lamellar spacing decreases with an increase in growth velocity. Figure 8 also shows that the simulated regular eutectic microstructures are in good agreement with the experimental results.[4]

It is to be noted that the present MCA model has an excellent computational efficiency. The computational time for the simulations in the present study was about $1\sim10$ h on a Pentium III PC of 1000 MHz.

IV. CONCLUSION

A modified cellular automaton (MCA) model has been developed and applied to investigate the microstructure evolution of the regular nonfaceted/nonfaceted lamellar eutectics using a model eutectic alloy and a transparent $CBr_4-C_2Cl_6$ eutectic alloy. The mechanisms of cooperative and competitive growth of two eutectic solid phases from a single liquid phase are incorporated into the numerical algorithm. The present model permits the prediction of arbitrarily complex eutectic growth modes, and the predicted eutectic microstructures effectively represent a wide range of realistic eutectic growth phenomena, such as eutectic oscillatory growth and the selection of eutectic lamellar spacing. The simulation results show that at a fixed growth velocity, there exists a stable growth lamellar spacing λ_m, which might be an optimum value with respect to the consideration of solute diffusion and curvature balance. When the initial lamellar spacing is smaller than the stable lamellar spacing, the eutectic lamellae adjust themselves to a new spacing by the

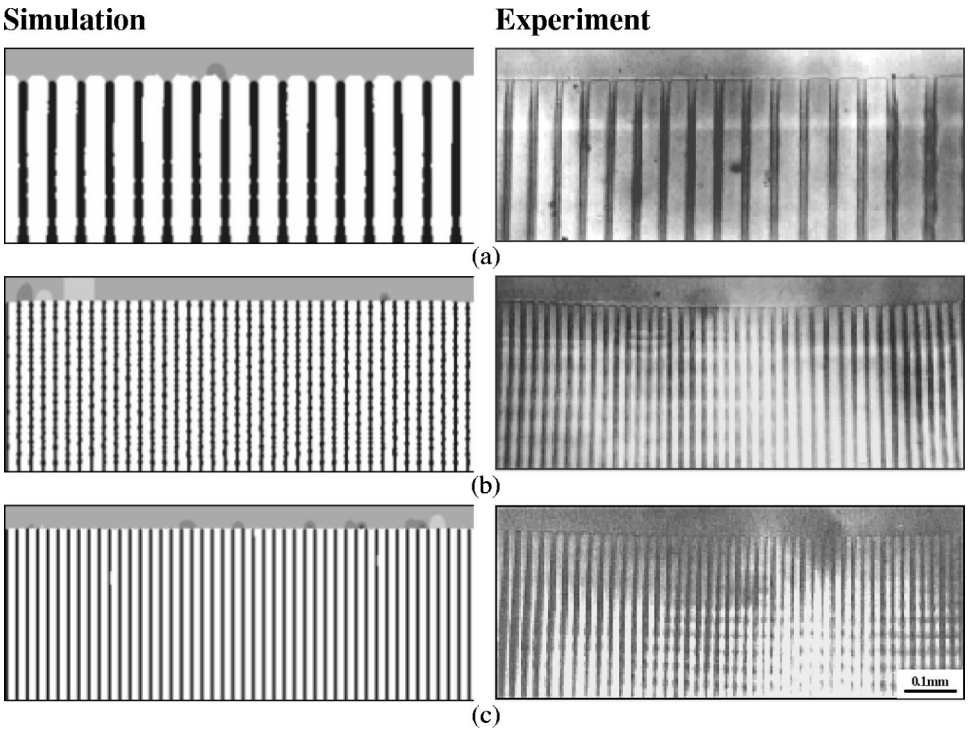

FIG. 8. The simulated and experimental (Ref. 4) steady-state eutectic growth morphology of a directionally solidified $CBr_4-8.4\,wt\,\%C_2Cl_6$ eutectic alloy with various growth velocities: (a) $v=0.2$ μm/s, (b) $v=0.5$ μm/s, and (c) $v=1.0$ μm/s.

elimination of lamellae. Conversely, when the initial lamellar spacing is larger than the stable lamellar spacing, solute rich pockets appear at the center of the α/liquid interface because of insufficient solute diffusion. At some larger initial lamellar spacing, unstable eutectic growth takes place, provoking the volume fraction adjustment by the branching of α lamellae. The stable growth lamellar spacing λ_m, which depends on the physical properties of the alloy, increases with an increase of solute diffusivity. Eutectic oscillatory growth is a consequence of the interaction between solute redistribution and volume fraction adjustments. The simulated steady-state eutectic microstructures with various growth velocities are in good agreement with the experimental results found in the literature.

ACKNOWLEDGMENTS

This work was financially supported by a Korea Research Foundation Grant (Grant No. KRF-2001-041-E00436).

*On leave from Department of Mechanical Engineering, Southeast University, Nanjing 210018, China.
†Electronic address: hong@yonsei.ac.kr

[1] V. Seetharaman and R. Trivedi, in *Solidification Processing of Eutectic Alloys*, proceedings of a symposium sponsored by the TMS Solidification Committee and the Powder Metallurgy Committee held at the TMS Fall Meeting, Cincinnati, Ohio, edited by D. M. Stefanescu, G. J. Abbaschian, and R. J. Bayuzick (TMS, Warrendale, PA, 1988), p. 65.
[2] A. Das and E.J. Mittemeijer, Metall. Mater. Trans. A **31A**, 2049 (2000).
[3] R. Trivedi and W. Kurz, in *Solidification Processing of Eutectic Alloys* (Ref. 1), p. 3.
[4] V. Seetharaman and R. Trivedi, Metall. Trans. A **19A**, 2955 (1988).
[5] J. Liu and R. Elliott, J. Cryst. Growth **148**, 406 (1995).
[6] J. Liu, Y. Zhou, and B. Shang, Acta Metall. Mater. **38**, 1625 (1990).
[7] J. Liu and R. Elliott, J. Cryst. Growth **162**, 107 (1996).
[8] E. Cadirli and M. Gunduz, J. Mater. Process. Technol. **97**, 74 (2000).
[9] U.S. Rai and R.N. Rai, J. Cryst. Growth **191**, 234 (1998).
[10] K.A. Jackson and J.D. Hunt, Trans. Metall. Soc. AIME **236**, 1129 (1966).
[11] R. Trivedi, P. Magnin, and W. Kurz, Acta Metall. **35**, 971 (1987).
[12] L.L. Zheng, D.J. Larson, Jr., and H. Zhang, J. Cryst. Growth **209**, 110 (2000).
[13] S.R. Coriell, G.B. McFadden, W.F. Mitchell, B.T. Murray, J.B. Andrews, and Y. Arikawa, J. Cryst. Growth **224**, 145 (2001).
[14] Ch.-A. Gandin and M. Rappaz, Acta Metall. Mater. **42**, 2233 (1994).
[15] I.S. Cho and C.P. Hong, ISIJ Int. **37**, 1098 (1997).
[16] K.Y. Lee and C.P. Hong, ISIJ Int. **37**, 38 (1997).
[17] Y.H. Chang, S.M. Lee, K.Y. Lee, and C.P. Hong, ISIJ Int. **38**, 63 (1998).
[18] S.Y. Lee, S.M. Lee, and C.P. Hong, ISIJ Int. **40**, 48 (2000).
[19] M.F. Zhu and C.P. Hong, ISIJ Int. **41**, 436 (2001).
[20] M.F. Zhu, J.M. Kim, and C.P. Hong, ISIJ Int. **41**, 992 (2001).
[21] M.F. Zhu and C.P. Hong, ISIJ Int. **42**, 520 (2002).
[22] J.M. Liu, Z.C. Wu, and Z.G. Liu, Scr. Mater. **38**, 715 (1998).
[23] L.L. Regel, W.R. Wilcox, D. Popov, and F. Li, Acta Astronaut. **48**, 101 (2001).
[24] D.I. Popov, L.L. Regel, and W.R. Wilcox, J. Cryst. Growth **209**, 181 (2000).
[25] B. Nestler and A.A. Wheeler, Physica D **138**, 114 (2000).
[26] A. Karma and A. Sarkissian, Metall. Mater. Trans. A **27A**, 635 (1996).
[27] M. F. Zhu and C. P. Hong (unpublished).
[28] M. F. Zhu, S. Nishido, and C. P. Hong, Int. J. Cast Metals Res. (to be published 2002).
[29] D. Stefanescu, *Science and Engineering of Casting Solidification* (Academic, New York, 2002), p. 188.
[30] P. Magnin, J.T. Mason, and R. Trivedi, Acta Metall. Mater. **39**, 469 (1991).
[31] L. Nastac, in *Proceedings of Modeling of Casting and Solidification Processes IV, Seoul, 1999*, edited by C. P. Hong, J. K. Choi, and D. H. Kim (Hanrimwon, Seoul, Korea, 2000), p. 31.
[32] P. Magnin and R. Trivedi, Acta Metall. Mater. **39**, 453 (1991).